

Analysis of Abdominal Fat Tissue Images Acquired with Continuously Moving Table MRI

S. Hadjidemetriou¹, J. Hennig¹, F. Klausmann¹, and U. Ludwig¹

¹Department of Diagnostic Radiology, University Hospital Freiburg, Freiburg, Germany

Introduction: The risk to develop disorders such as hypertension, diabetes, and hyperlipidemia have been shown to correlate intimately with the amount of visceral fat in the abdomen [1,2]. In this work the abdominal fat was imaged in high contrast with a continuously moving table whole body MRI technique. A method is presented that allows the repeatable and reliable analysis of the imaged abdominal lipids into subcutaneous and visceral. The data is pre-processed to restore intensity uniformity [3]. The corrected images are analyzed with the graph cuts algorithm [4] operating on level sets to extract the body region. Then, the contour between the subcutaneous and visceral fat regions is identified with the graph cuts operating on a simulated random walks potential [5]. The method provides the subcutaneous fat in an unsupervised manner, is able to represent the variable fat content of different visceral regions, and is robust to noise or artifacts exterior to the body.

Subjects and imaging: 11 volunteers, 10 men and 1 woman (average age 30 ± 10 y) were examined on a 1.5Tesla scanner (Magnetom Espree, Siemens Medical Solutions, Erlangen). A continuously moving table (CMT) double echo gradient echo sequence with a flip angle $FA=70^\circ$, $TE1=2.38$ ms and $TE2=4.76$ ms was used. The FOV was adapted to the size of the volunteer and varied between 310mm and 392mm in phase direction (FOV in read direction=450mm). This resulted in various repetition times $TR=93$ -139ms with a matrix size of 320×259 . The slice thickness was 5mm without slice spacing. Three surface coils were used with GRAPPA acceleration of 2. On average 64 slices were acquired to ensure coverage of the abdominal region. All abdominal measurements were taken in the exhaled position. A two-point DIXON reconstruction provided a water and a fat image.

Image analysis: The fat DIXON image I_{DF} is smoothed with median filtering and then restored for intensity uniformity in terms of non-parametric statistics [3]. An example is shown in Fig. 1. The non-zero mean noise in the background of the restored image is represented with a Rayleigh distribution. The largest connected component in the remaining image region provides the foreground fat signal I_F . The difference between I_{DF} and I_F gives the non-signal region I_B corresponding to air or organs without fat content.

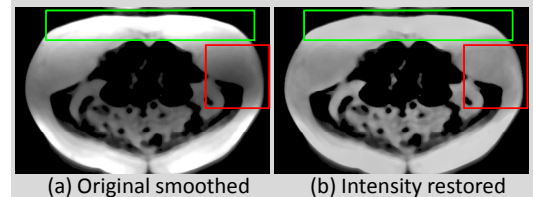


Fig. 1: Original and intensity restored slices with the same average intensity. Green is a bright and red is a dark window in the original.

The first segmentation step processes the fat region I_F to estimate the outer surface of the abdomen, which predominantly coincides with the outer surface of the subcutaneous fat. However, some body regions such as the spinal cord of thin subjects may not be covered with subcutaneous fat and thus the interior and exterior background can come in contact. The seed region for the abdomen is image I_F . The seed region for the exterior of the body is a narrow frame I_M inscribed to the image boundary. The graph cuts are applied to a smooth distance map computed between the two seed regions with I_F fixed to maximum and I_M fixed to zero. The distance computation involves the curvature so that the distance increases faster at concave points. The segmentation provides the image region occupied by the abdomen I_{ABD} . The difference between I_{ABD} and the fat signal I_F gives the visceral background I_{BV} . The remaining background region $I_B - I_{BV}$ provides the background out of the body, I_{BO} . An example is shown in Fig. 2(a-c).

The second segmentation step provides the inner boundary of the subcutaneous fat in contact with the visceral fat region. The graph cuts algorithm is also used [4]. The seed for the visceral region is I_{BV} and for the subcutaneous region is I_{BO} . The graph cuts are applied to a simulated potential field computed with the random walks algorithm [5] between the seed I_{BO} fixed to zero and the seed I_{BV} fixed to maximum. The variation of the potential is low within both the subcutaneous and the visceral fat regions, but is high at the border between them. The segmentation provides the visceral region, I_V . The difference between I_V and I_{ABD} gives the subcutaneous fat I_{FS} . The difference between I_{FS} and I_F provides the visceral fat image I_{FV} . An example of this segmentation step is shown in Fig. 2(d-f) and of visualizations are depicted in Fig. 2(g-h).

The cost of both segmentation steps is lowered by extending the seeds of the corresponding interior region with an ellipse centered at the mean seed position. The size of the ellipses is limited so that they lie within the seed regions. The interior seeds are I_F in the first segmentation and I_{BV} in the second segmentation. The implementation of the method is in C++, it uses the ITK Kitware library, and the 3D Slicer software package.

Results and discussion: The visceral and subcutaneous abdominal regions were successfully segmented from the 11 DIXON images. The intensity restoration algorithm is non-parametric and can represent the variable fat occupancies of the voxels in the visceral region efficiently without assuming a finite number of classes [1]. The cost of the segmentations of the relatively large abdominal volumes can be lowered by considering only a region of interest that includes the contours to be detected. The segmentations can also support a variable topology and thus increase the robustness to noise or artifacts exterior to the body compared to methods based on active contours [1]. Despite the variable topology, this method is able to properly identify the visceral region and the contained fat by first resolving contacts between the visceral background and the out of the body background.

References:

- [1] Positano, V., Cusi, K., Santarelli, M.F., Sironi, A., Petz, R., DeFronzo, R., Landini, L., Gastaldelli, A., JMRI, 28, (2008)
- [2] Kullberg, J., Johansson, L., Ahlstrom, H., Courivaud, F., Koken, P., Eggert, H., Bornert, P., JMRI, 30, (2009)
- [3] Hadjidemetriou, S., Studholme, C., Mueller, S., Weiner, M., Schuff, N., Medical Image Analysis, 13 (1), (2009)
- [4] Boykov, Y., Lev, G.: Graph cuts and efficient N-D image segmentation, IJCV, 70(2), (2006)
- [5] Grady, L.: Random walks for image segmentation, IEEE Trans. on PAMI, 28(11), (2006)

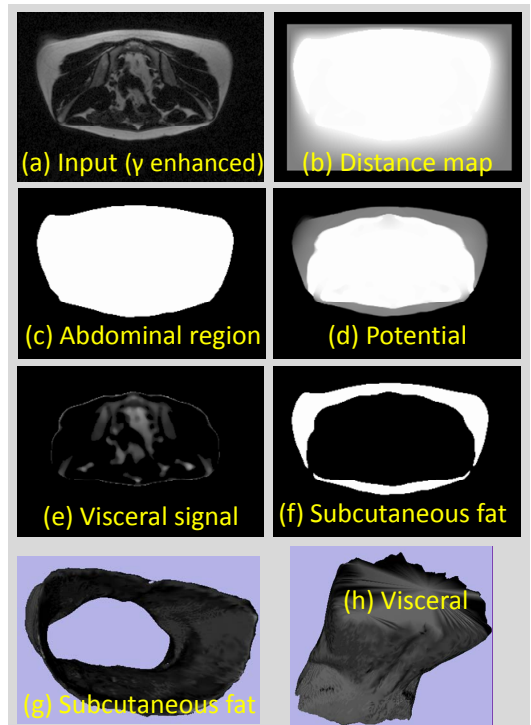


Fig. 2: Images (b-c) are from the first segmentation, (d-f) from the second segmentation, and (g-h) are surface renderings.